Article

The Effect of Skelp Thickness on Precipitate Size and Morphology for X70 Microalloyed Steel Using Rietveld Refinement (Quantitative X-ray Diffraction)

Corentin Chatelier [1,2,†], J. Barry Wiskel [1,*], Douglas G. Ivey [1] and Hani Henein [1]

[1] Department of Chemical and Materials Engineering, University of Alberta, Edmonton, AB T6G 2V4, Canada; chatelie@ualberta.ca or corentin.chatelier@univ-lorraine.fr (C.C.); divey@ualberta.ca (D.G.I.); henein4876@killamtrusts.ca (H.H.)

[2] Mines Nancy, Université de Lorraine, Campus Artem, 92 rue Sergent Blandan, F-54000 Nancy, France

* Correspondence: bwiskel@ualberta.ca; Tel.: +1-780-492-6178; Fax: +1-780-492-2881

† Current address: Institut Jean Lamour, Université de Lorraine F-54000 Nancy, France and Synchrotron SOLEIL, F-91190 Saint-Aubin, France.

check for updates

Abstract: Precipitates in thin-walled (11 mm) and thick-walled X70 (17 mm) microalloyed X70 pipe steel are characterized using Rietveld refinement (a.k.a. quantitative X-ray diffraction (QXRD)), inductively coupled plasma mass spectrometry (ICP), and energy-dispersive X-ray spectroscopy (EDX) analyses. Rietveld refinement is done to quantify the relative abundance, compositions, and size distribution of the precipitates. EDX and ICP analyses are undertaken to confirm Rietveld refinement analysis. The volume fraction of large precipitates (1 to 4 µm—mainly TiN rich precipitates) is determined to be twice as high in the thick-walled X70 steel (0.07%). Nano-sized precipitates (<20 nm) in the thin-walled steel exhibit a higher volume fraction (0.113%) than in the thick-walled steel (0.064%). The compositions of the nano-sized precipitates are similar for both steels.

1. Introduction

Microalloyed steels are a type of high strength, low alloy steel containing additions of carbon (C), nitrogen (N), niobium (Nb), titanium (Ti), and/or vanadium (V) in amounts less than 0.1 wt %. These steels may also contain molybdenum (Mo) and chromium (Cr) in amounts exceeding 0.1 wt %. Microalloyed steels are widely used in the pipeline industry [1,2] due to their good strength, weldability, and toughness. Strengthening is achieved primarily via grain size reduction, but precipitation of second phase particles can also contribute to the strength of the steel [3–5]. Precipitation strengthening can be calculated by the following equation [6]:

$$\sigma_{ppt}(\text{MPa}) = \left(\frac{10.8 V_f^{1/2}}{X}\right) \ln\left(\frac{X}{6.125 \times 10^{-4}}\right) \tag{1}$$

where V_f is the volume fraction of precipitates and X is the mean diameter (µm) of the precipitates. Changing the steel composition and/or processing conditions affects the value of both V_f and X and, ultimately, the mechanical properties of the steel. Therefore, the ability to quantify precipitate characteristics is important.

The volume fraction of precipitates in microalloyed steels is very low ($\approx$0.1%), and the size of some of the precipitates can be very small (less than 10 nm). Conventional characterization techniques,

such as scanning electron microscopy (SEM) [7] or transmission electron microscopy (TEM) [3], can be used, but it is difficult and/or time consuming to obtain statistically relevant information. The size distribution of precipitates and volume fraction of nano-sized precipitates can also be determined using small angle neutron scattering (SANS) [8–10]. However, neither the chemical composition nor the morphology can be easily determined using SANS. A supplemental precipitate quantification technique, such as Rietveld refinement of X-ray diffraction (XRD) patterns, is needed to properly characterize precipitates in microalloyed steels.

To analyze precipitates using Rietveld refinement, it is necessary to extract the precipitates from the steel using a matrix dissolution technique [11,12]. Precipitate extraction allows for the analysis of a statistically significant number of precipitates. In addition, the extracted precipitates can be characterized using other analytical techniques, such as SEM coupled with energy dispersive X-ray (EDX) analysis.

The Rietveld method, in conjunction with XRD, which is commonly referred to as quantitative XRD (QXRD), is a characterization methodology that calculates a theoretical XRD pattern and matches it with the experimental diffraction pattern [13,14]. A number of different parameters are used to calculate the theoretical pattern including the lattice parameter(s) of each phase, the atomic composition(s), the crystallite size (L_{vol} in nm), the lattice strain (ε_o), and the relative abundance (weight and/or volume fraction) of precipitates. The value of L_{vol} is related to the mean precipitate radius (R) by the following equation [15]:

$$L_{vol} = \frac{3 \cdot R \cdot (1 + c)^3}{2} \tag{2}$$

where $c = 0$ for a monodisperse spherical distribution and $c = 0.2$ for a typical lognormal distribution [16]. A lognormal distribution ($c = 0.2$) was assumed during precipitate analysis. QXRD has been successfully applied to precipitate analysis in Grade 100 steel [12].

2. Materials and Methods

2.1. Steels Analyzed

Conventional 11 mm thick X70 steel (X70) and a 17 mm thick X70 steel (TWX70) skelp were analyzed in this work. The mechanical properties (yield strength, ultimate tensile strength, and percentage of elongation) and composition of each steel are shown in Table 1. The X70 and TWX70 steels have very similar processing conditions (similar finish rolling temperature ($\approx$800 °C) and runout table cooling rates ($\approx$15 °C/s)). The primary difference between the two steels is the thickness and variations in the C, Nb, Mo, and Cr content. The skelp thickness does not markedly affect the mechanical properties of the steels (less than 5% difference for the yield and ultimate tensile strength). Both steels are within the specifications of X70 steels.

Table 1. Composition of X70 and TWX70 steels.

Steel	Thickness	YS	UTS	%El	C	N	Nb	Mo	Ti	Cr	V
	(mm)	(MPa)	(MPa)		(wt %)	ppm	(wt %)	(wt %)	(wt %)	(wt %)	(wt %)
X70	11	524.0	651.6	37	0.052	70	0.09	0.13	0.016	0.23	0.003
TWX70	17	554.3	679.1	38	0.043	90	0.07	0.19	0.016	0.09	0.003

2.2. Matrix Dissolution and Precipitate Collection

A mixture of 6N HCl and distilled water, according to ASTM standard E194-90 [17], was used to dissolve samples of each steel. The samples were taken from the full thickness of the skelp. Table 2 summarizes the initial weight of each sample, the volume of solution used, the dissolution temperature, the time for dissolution, and the weight of residue collected.

Table 2. Dissolution parameters for X70 and TWX70 steels.

Steel	Weight Steel	Volume Solution	T	Time	Weight Residue
	(g)	(mL)	(°C)	(weeks)	(mg)
X70	48.1474	2500	90	3	67.1
TWX70	10.1308	500	90	1	12.2

Lu [3] observed the presence of amorphous SiO_2 in the residues using a similar dissolution technique to that described in this work. The amorphous phase presented difficulties in subsequent SEM/TEM and QXRD analyses. To remove dissolved O_2 from the dissolution system (and prevent the formation of the silica), N_2 was directly injected into the solution before starting and during the dissolution process. This procedure reduced the amount of amorphous SiO_2 collected in the residues [18]. Following complete dissolution, the solution was centrifuged (to separate the liquid from the solid residues) using a Sorvall RC-6 centrifuge (Mandel) operating at a speed of 18,300 RPM. The residue free liquid was then analyzed using inductively coupled plasma mass spectrometry (ICP), and the solid residues were analyzed using XRD and EDX analysis in the SEM.

2.3. ICP Analysis of the Supernatant Solution

Inductively coupled plasma (ICP) mass spectroscopy (Perkin Elmer Elan 6000 ICP-MS, Waltham, MA, USA) was used to measure the concentration of alloying elements (Ti, Nb, Mo, Cr, etc.) that remained (i.e., were not present as precipitates) in the dissolution solution. Calibration of the ICP system was undertaken using a four point calibration method [18]. Based on the mass of the steel sample and the volume of the initial solution, the mass fraction of each element dissolved in the solution was calculated. This information was used to complete the mass balance for the quantitative XRD analysis of the collected precipitates and will be discussed in a subsequent section.

2.4. XRD of the Solid Residue

A Rigaku Ultima IV diffractometer was used to obtain diffraction patterns from the residues. As the amount of residue collected was quite low ($\approx$5–10 mg per 10 g of steel), a quartz sample holder was used to minimize diffraction issues related to sample thickness. Table 3 provides the X-ray diffraction parameters used. A LaB_6 standard was used to calibrate instrument broadening.

Table 3. X-ray diffraction parameters.

Parameter	Value
Radiation	Cobalt
Detector	D/Tex with Fe filter
2θ range	5–100°
Scan	0.02°/step
Scan speed	2°/min

2.5. Rietveld Refinement and Analysis

Rietveld refinement was undertaken for each diffraction pattern using TOPAS Academic Software [19] (4.1, Bruker AXS Inc., Madison, WI, USA, 2007). This software uses a linear least squares method to predict the measured X-ray diffraction pattern. The parameters used in the fitting calculation include the lattice parameters for each phase, the occupancy of each atom in the unit cell, the scale factor (relative intensity of each phase), and the effects of crystallite size (L_{vol}) and strain. The goodness of the fit was evaluated using the lower weighted profile R-factor, R_{wp} [20].

The relative weight fraction (W_j) of each phase (i.e., precipitate type) observed in the diffraction pattern was calculated using Equation (3) [21].

$$W_j = \frac{S_j \cdot M_j \cdot Z_j \cdot V_j}{\sum_{i=1}^{n} S_i \cdot M_i \cdot Z_i \cdot V_i} \tag{3}$$

where S is the scale factor calculated by TOPAS, n is the number of phases, M is the mass of the unit cell, Z is the number of atoms in the unit cell, and V is the unit cell volume of the phase. Using the relative weight fraction and atomic occupancy of each phase, it was possible to calculate the total amount of each element in all the precipitate types. The mass fraction of each element that remained in solution (i.e., the elements not in precipitate form) was then calculated and compared to the ICP results. From the value of crystallite size (L_{vol}), the mean radius R of a particular precipitate type was calculated using Equation (2).

2.6. SEM-EDX Analysis of Collected Precipitates

A Zeiss FE-SEM was used to image the precipitates collected in the residue. A Bruker EDX system was utilized to analyze the composition of each precipitate. In order to improve imaging of the fine precipitates, a low accelerating voltage (between 5 and 10 kV) was used. Samples were coated with a thin layer of carbon to minimize charging. For the composition analysis, an accelerating voltage of 20 kV was used.

A major issue with SEM-EDX analysis was that the fine precipitates tended to agglomerate on drying. A suspension of ethanol and residue was prepared using ultrasonic vibration. A small amount of the suspension was place on carbon tape. Once the ethanol evaporated, the individual precipitates remaining on the tape were analyzed. In total, using this technique, 82 nano-sized precipitates were analyzed for the X70 steel and 112 nano-sized precipitates were analyzed for the TWX70 steel [18].

3. Results

3.1. ICP Results

Based on the nominal composition (Table 1), the initial weight of the sample, and the mass fraction of each element dissolved in the solution determined by ICP, the wt % of each element present in solid solution in the original steel sample or in precipitate form was calculated. Figure 1 graphically illustrates the amount of each element either in solid solution or in precipitate form for both X70 and TWX70. For the X70 steel (Figure 1a), the amounts of Nb and Ti remaining in solution are relatively low (compared with the nominal composition). Conversely, most of the Cr and V remain in solution. A small amount of the Mo is in precipitate form, but the majority remains in solution. For the TWX70 steel (Figure 1b), the amounts of Nb and Ti remaining in solution are relatively low (compared with the nominal composition), and most of the Cr and V remains in solution. As with the X70 steel, a small amount of the Mo is in precipitate form, but the majority remains in solution.

3.2. SEM Size Analysis

Figure 2 shows an SEM image of individual precipitates (circled in green) that were retained on the carbon tape following evaporation of the ethanol and precipitate suspension described in Section 2.6. Small agglomerates of precipitates (circled in red) are also observed. For the purpose of this work, only the size of the individual precipitates was measured.
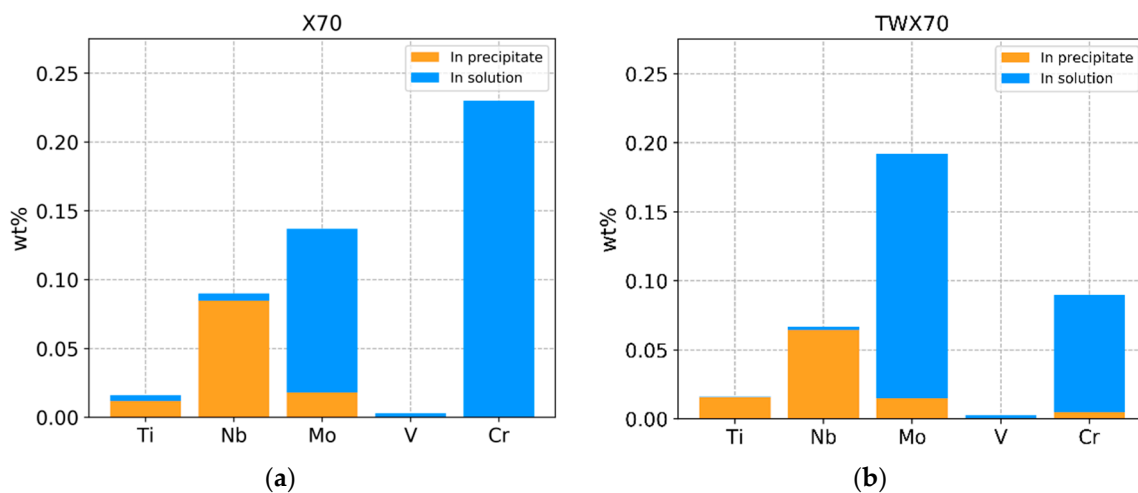
Figure 1. Composition in (wt %) of each element either in solid solution or in precipitate form for (**a**) X70 steel and (**b**) TWX70.
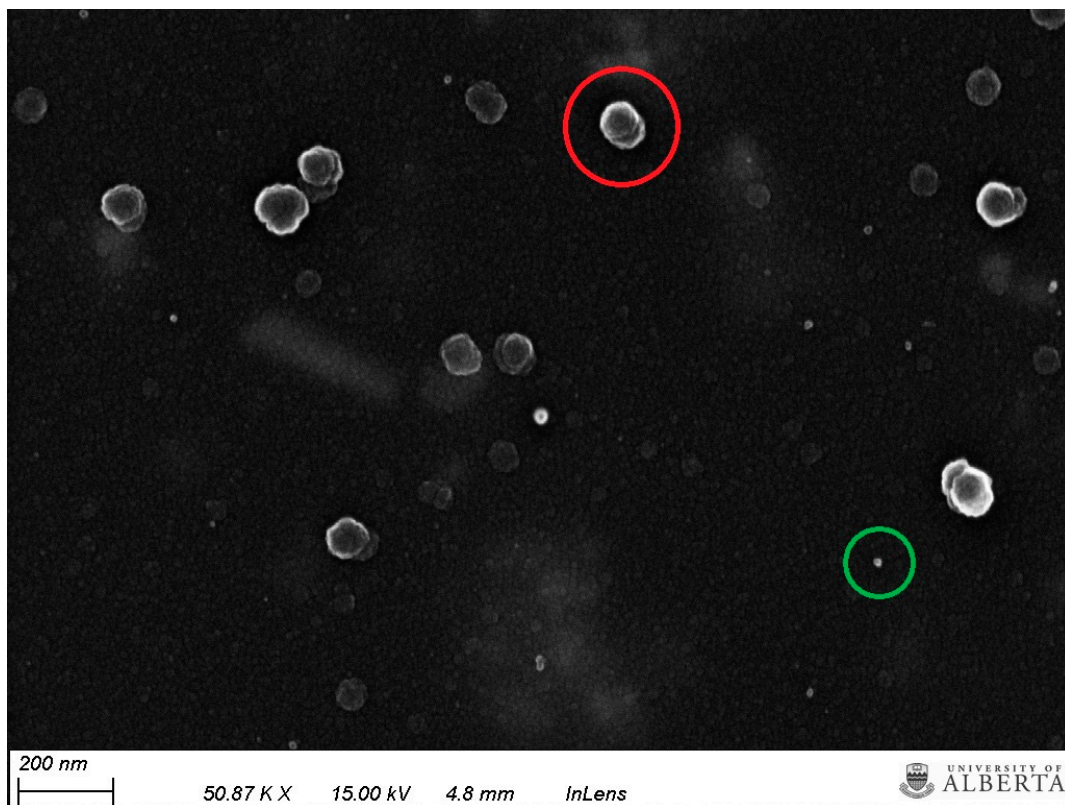
Figure 2. SEM secondary electron (SE) image of precipitates retained on carbon tape for X70 steel. An individual particle is circled in green while an agglomerate is circled in red.

Figure 3a shows the measured size distribution of precipitates extracted from the X70 steel and Figure 3b shows the size distribution of precipitates from the TWX70 steel. For the X70 steel, the average size of the fine precipitates is 7.95 nm with a standard deviation of 2.19 nm. The maximum size measured was 15.2 nm and the minimum size was 3.6 nm. For the TWX70 steel, two overlapping distributions were observed. The average size of the finer distribution was 4.4 nm and the average size of the larger precipitate distribution was 10 nm, with a maximum size measured of 13.9 nm. The overall average size was 9.15 nm.

(a)   (b)
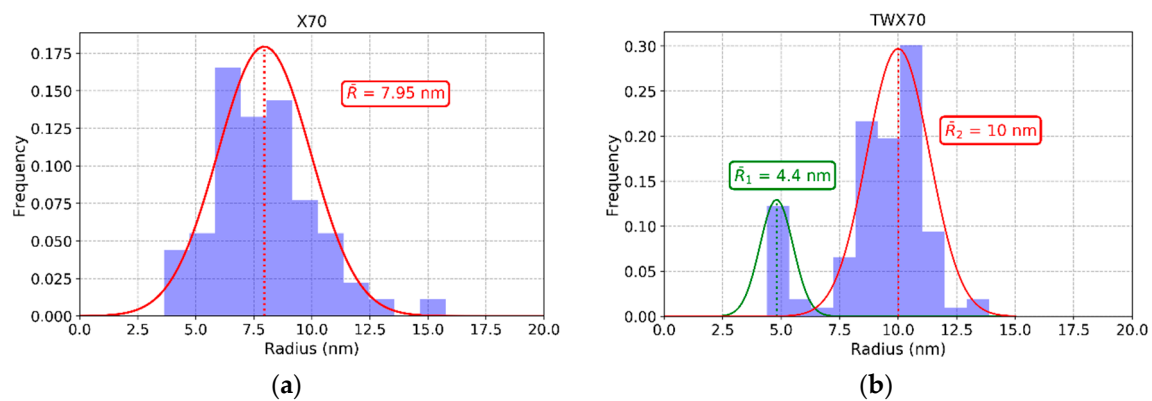
Figure 3. Measured size distributions of nano-sized precipitates from SEM images for (**a**) X70 steel (82 particles) and (**b**) TWX70 steel (112 particles).

3.3. Composition Analysis

The composition of individual precipitates was determined using SEM-EDX analysis. Figure 4 shows the atomic fraction of Nb, Ti, and Mo measured for both fine and large (µm scale) particles for the X70 steel. The large precipitates are Ti-rich, while the fine (nano) precipitates are composed primarily of Nb with some Mo and Ti. For both precipitate sizes, Nb replaces Ti in the precipitate structure. The atomic fraction ranges from 0.95 to 0.75 Ti for the large precipitates, while the fine precipitates exhibit a Nb atomic fraction range from 0.55 to 0.93, with the majority >0.7 Nb. The Mo present in the fine precipitates is relatively constant at an atomic fraction of ≈0.05 and is relatively independent of the Ti atomic fraction. The Mo content of the large precipitates is virtually nil.
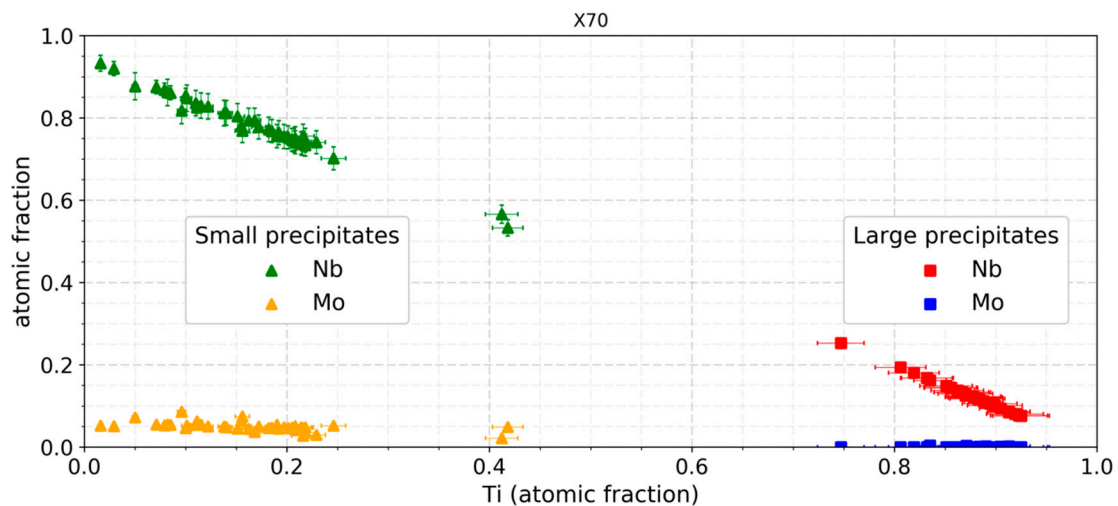
Figure 4. Atomic fraction of X70 steel precipitates measured using EDX analysis.

Figure 5 shows the atomic fraction of Nb, Ti, and Mo, measured for both fine and large (µm scale) precipitates for TWX70 steel. As observed for the X70 steel, the large precipitates are Ti-rich, while the fine (nano) precipitates are composed primarily of Nb, with lower levels of Mo and Ti. The atomic fraction of the large precipitates ranges from 0.95 to 0.75 Ti. The fine precipitates exhibit a Nb atomic fraction range from 0.4 to 0.83; however, unlike the X70 steel, the nano-sized precipitates exhibit two groupings of composition. In one grouping, there is range of Nb atomic fractions (0.4 to 0.8) with Ti content decreasing as Nb content increases, and the Mo content is relatively constant at an atomic fraction of ≈0.10. In the second grouping (circled in Figure 6), the Mo content is significantly higher, i.e., with an atomic fraction ranging from 0.22 to 0.28, accompanied by a lower Nb content

(0.52 to 0.56 atomic fraction). The presence of the second grouping of precipitates is attributed to the higher Mo content and lower Nb content of the TWX70 steel (Table 1).
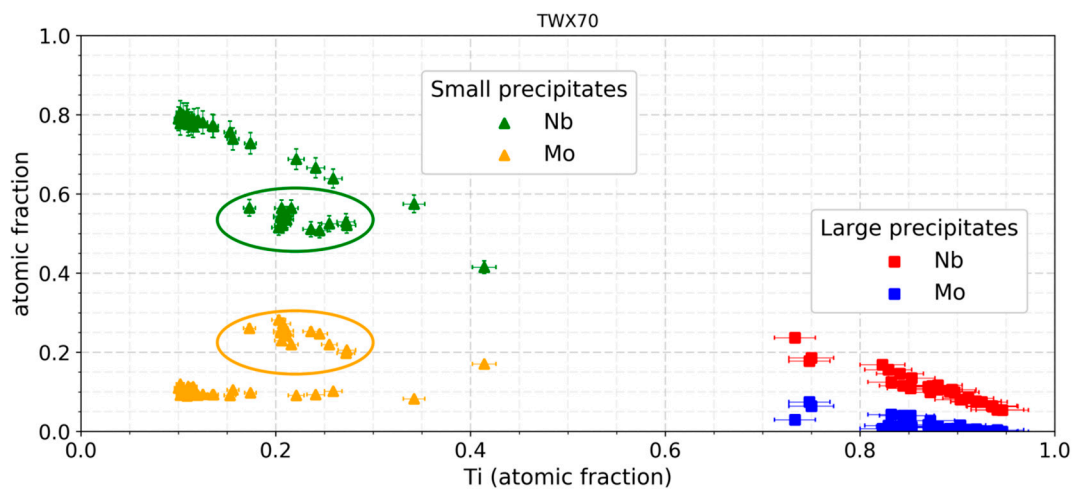
Figure 5. Atomic fraction for TWX70 steel precipitates measured using EDX analysis.

3.4. X-ray Diffraction

An XRD pattern of the residue collected from the X70 steel in shown in Figure 6. The relatively small and broad peak at $2\theta \approx 27°$ is attributed to a small amount of amorphous SiO_2. Couplets of peaks (a large intensity peak followed by a significantly less intense diffraction peak) are observed throughout the diffraction pattern. The large first peak is associated with a Nb/C-rich precipitates, whereas the second (and smaller) peak in each set is associated with Ti/N-rich precipitates. Both peaks in each couplet are characteristic of a NaCl-type structure (Fm3m space group). The diffraction planes (e.g., (111)) for each couplet are included in Figure 6.
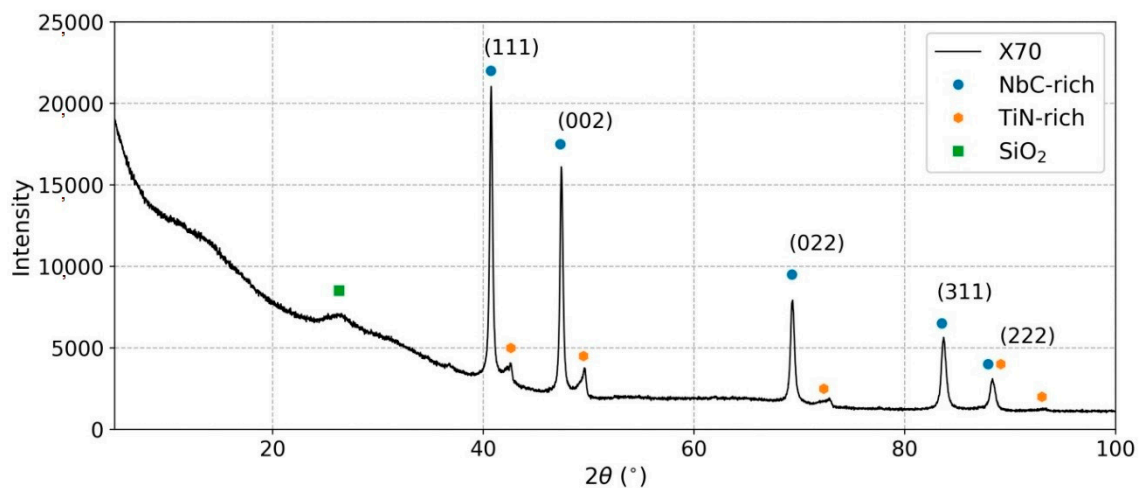
Figure 6. XRD pattern from X70 steel residue.

Figure 7 shows the measured XRD pattern of the collected residue for TWX70 steel. As with the X70 steel, couplets of diffraction peaks are observed throughout the diffraction pattern and are associated with Nb/C-rich precipitates and Ti/N-rich precipitates, respectively.
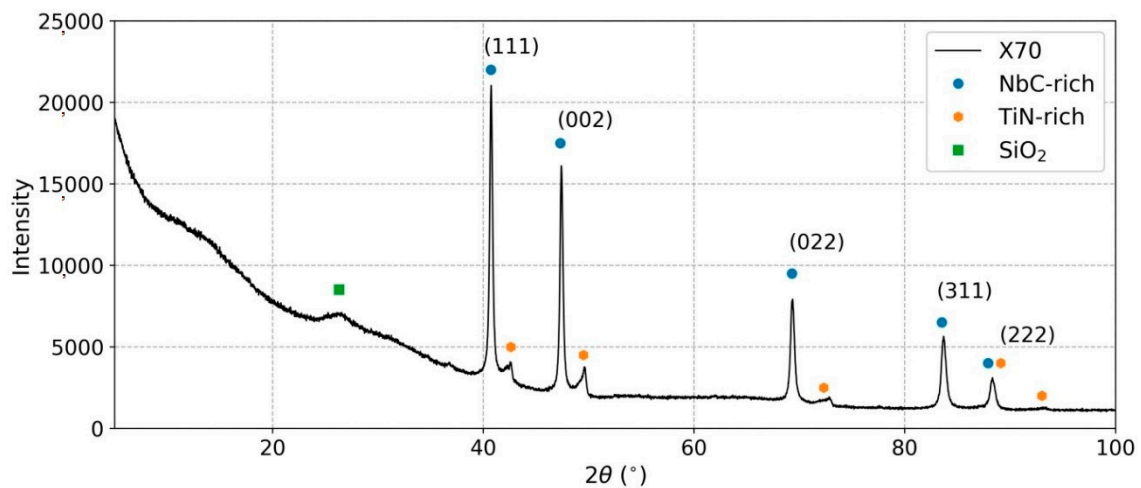
Figure 7. XRD pattern from TWX70 steel residue.

3.5. Rietveld Refinement

3.5.1. Rietveld Refinement of X70 Steel

The measured and predicted diffraction patterns for X70 are shown in Figure 8. Reasonably good agreement between the predicted and measured diffraction patterns is observed and confirms the veracity of the refinement. Included in the figure are short vertical lines which indicate the 2θ position of each peak (for each different diffracting plane) for each of the precipitate types (inset) included in the refinement. Seven types of precipitates were chosen for the fitting of the Ti/N rich diffraction peak to account for the variation in Nb and Ti atomic fraction observed in the large (TiNb)CN precipitates (Figure 4).
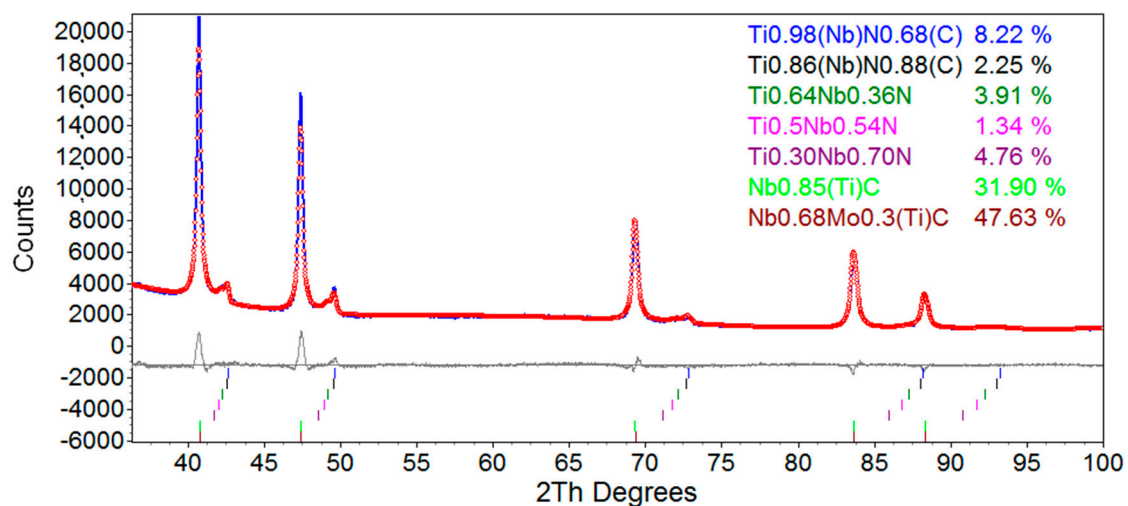
Figure 8. Comparison between measured and predicted diffraction patterns for X70 steel.

A summation of the refinement details for each precipitate type is shown in Table 4. Included in this table are the lattice parameters a (based on the 2θ peak position), the values of microstrain (ε_o) and L_{vol}, the calculated precipitate radii (based on Equation (2)), and the wt % of each precipitate type in the residue. Microstrain (or inhomogeneous strain) within the crystal lattice arises from local atomic positional distortions due to the presence of defects such as dislocations, solid solution elements, and vacancies. The microstrain levels measured for both X70 steel and TWX70 steel are relatively low. $L_{vol} = 4000$ nm does not represent the actual precipitate size and is the default value for the

refinement program when the size of the precipitates are relatively large. The most common type of precipitate (by wt %) is nano-sized $Nb_{0.68}Mo_{0.30}Ti_{0.02}C$, followed by the slightly larger, but still nano-sized, $Nb_{0.85}Ti_{0.15}C$. These two types of precipitates account for almost 80% of the residue in the X70 steel.

Table 4. Refinement results for X70 steel.

Atomic Composition	a (Å)	ε_o (%)	L_{vol} (nm)	R (nm)	wt (%)
$Ti_{0.97}Nb_{0.03}(N_{0.68}C_{0.32})$	4.26 ± 0.02	0.14 ± 0.02	4000	-	8.2 ± 1.2
$Ti_{0.86}Nb_{0.14}(N_{0.88}C_{0.12})$	4.27 ± 0.04	0.19 ± 0.03	4000	-	2.3 ± 0.3
$Ti_{0.64}Nb_{0.36}N$	4.30 ± 0.04	0.19 ± 0.03	4000	-	3.9 ± 0.6
$Ti_{0.50}Nb_{0.50}N$	4.32 ± 0.04	0.28 ± 0.04	4000	-	1.3 ± 0.2
$Nb_{0.70}Ti_{0.30}N$	4.35 ± 0.04	0.82 ± 0.12	4000	-	4.8 ± 0.7
$Nb_{0.85}Ti_{0.15}C$	4.45 ± 0.05	0	40.3 ± 6.1	15.6 ± 2.3	31.9 ± 4.8
$Nb_{0.68}Mo_{0.30}Ti_{0.02}C$	4.45 ± 0.05	0	10.9 ± 1.6	4.2 ± 0.6	47.6 ± 7.1

3.5.2. Rietveld Refinement of TWX70 Steel

The measured and predicted diffraction patterns for TWX70 steel are shown in Figure 9. The reasonably good agreement (except for the Ti/N-rich peak at $2\theta = 49.5°$) between the predicted and measured diffraction patterns confirms the veracity of the refinement. Included in the graph are short vertical lines which indicate the 2θ position of each peak (for each different diffracting plane) for each of the precipitate types (inset) included in the refinement. Six types of precipitates were chosen for the fitting of the Ti/N rich diffraction peak to account for the variation in Nb and Ti atomic fraction observed in the large (TiNb)CN precipitates (Figure 5).
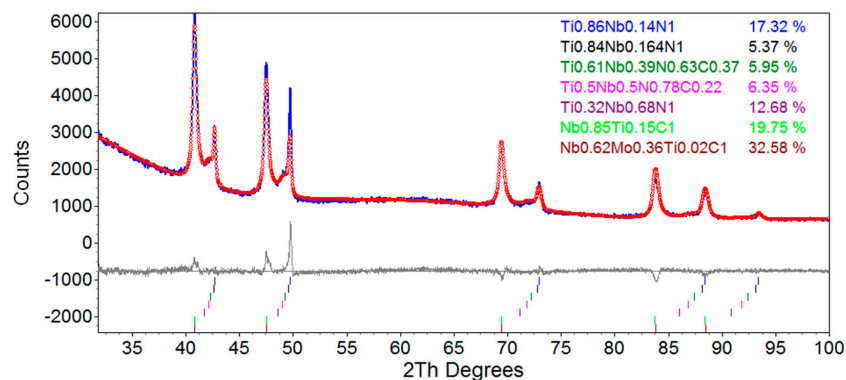
Figure 9. Comparison between measured and predicted diffraction patterns for X70 steel.

A summation of the refinement details for each precipitate type is shown in Table 5. The most common type of precipitate (by wt %) is nano-sized $Nb_{0.68}Mo_{0.30}Ti_{0.02}C$, followed by the slightly larger $Nb_{0.85}Ti_{0.15}C$ and $Ti_{0.86}Nb_{0.14}N$. Unlike the X70 steel, the former two precipitate types only account for just over 50% of the residue weight. The nitrides are much more prevalent in the TWX70 residue.

Table 5. Refinement results for TWX70 steel.

Atomic Composition	a (Å)	ε_o (%)	L_{vol} (nm)	R (nm)	wt (%)
$Ti_{0.86}Nb_{0.14}N$	4.26 ± 0.02	0.10 ± 0.02	4000	-	17.3 ± 2.6
$Ti_{0.84}Nb_{0.16}N$	4.27 ± 0.04	0.23 ± 0.03	4000	-	5.4 ± 0.8
$Ti_{0.61}Nb_{0.39}(N_{0.63}C_{0.37})$	4.29 ± 0.04	0.25 ± 0.04	4000	-	5.9 ± 0.9
$Ti_{0.50}Nb_{0.50}(N_{0.78}C_{0.22})$	4.32 ± 0.04	0.27 ± 0.04	4000	-	6.4 ± 1.0

Table 5. *Cont.*

Atomic Composition	a (Å)	ε_o (%)	L_{vol} (nm)	R (nm)	wt (%)
$Nb_{0.68}Ti_{0.32}N$	4.35 ± 0.04	0.99 ± 0.15	4000	-	12.7 ± 1.9
$Nb_{0.84}Ti_{0.16}C$	4.44 ± 0.05	0	28.9 ± 4.3	11.2 ± 1.7	19.8 ± 2.9
$Nb_{0.62}Mo_{0.36}Ti_{0.02}C$	4.44 ± 0.05	0	13.2 ± 2.0	5.1 ± 0.8	32.6 ± 4.9

3.6. Lattice Parameter Comparison

The measured lattice parameters provided by the refinement (Tables 4 and 5) are compared to the predicted lattice parameter values based on a linear interpolation (Vegard's law) between the known lattice sizes of NbC and TiC, and NbN and TiN, as a function of Ti concentration. The red line in Figures 10a and 10b represents the variation in lattice parameter of $(Ti_xNb_{(1-x)})C$ as a function of Ti content (i.e., the value of x). The blue line in each figure represents the variation in lattice parameter of $(Ti_xNb_{(1-x)})N$ as a function of Ti content (i.e., the value of x). The lattice parameters predicted by Rietveld refinement, for particular precipitate atomic compositions (represented by filled circles), agree reasonably well with the interpolated lattice parameter values. The only exception is for the smallest precipitates (i.e., predicted atomic fraction of Ti is <0.05) where Mo is present in the structure.
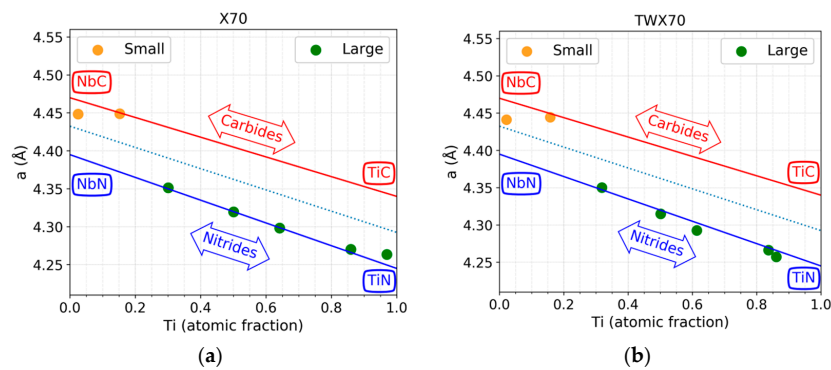
Figure 10. Lattice parameter as a function of Ti content for (**a**) X70 steel and (**b**) TWX70 steel.

4. Discussion

4.1. Mass Balance of Elements: Comparison between ICP and QXRD

A mass balance comparison, between the ICP data and the relative amount and atomic composition of each precipitate type calculated through Rietveld refinement, for Ti, Nb, and Mo was undertaken (Figure 11). The amount of each element in the precipitates from Rietveld refinement was calculated based on the size of the steel sample, the weight of the residue, the atomic composition, and the wt % determined by Rietveld refinement (Tables 4 and 5). The ICP measurements independently confirm the veracity of Rietveld refinement in determining the element distribution in the precipitates for microalloyed steels.
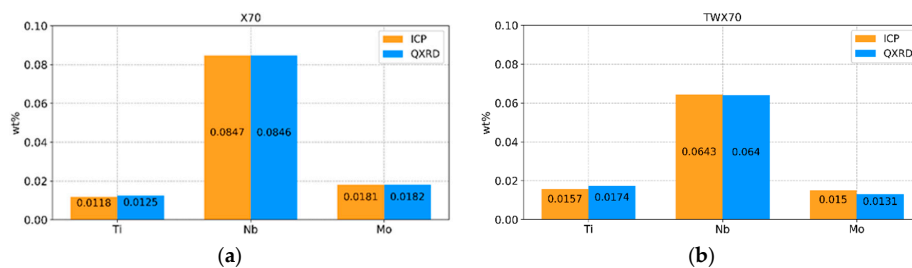
Figure 11. Comparison of Ti, Nb, and Mo amounts in precipitates for ICP and QXRD for (**a**) X70 steel and (**b**) TWX70 steel.

4.2. Nano Sized Precipitates

The sizes and atomic compositions (Nb, Mo, and Ti) of the nano-scale precipitates measured using SEM-EDX analysis are compared with Rietveld refinement values in Table 6. The mean size of the precipitates measured by SEM imaging for X70 steel was 7.95 nm, with the range of values extending from 3.6 to 15.2 nm. The distribution of measured precipitate sizes is similar to the nano precipitate sizes predicted by Rietveld refinement (4.2 nm and 15.6 nm). The mean sizes of nano-scale precipitates measured by SEM for TWX70 steel were 4.4 and 10.0 nm, with the range of values extending from 4.4 to 13.9 nm. The distribution of measured precipitate sizes correlates with the nano precipitate sizes predicted by Rietveld refinement (5.1 nm and 11.2 nm). The reasonable agreement between the SEM-measured values and those predicted by Rietveld refinement indicates that the latter technique is suitable for quantifying the mean size of nano-sized precipitates in microalloyed steels. The disadvantage of Rietveld refinement measurements is that only a mean value is provided (not a distribution). Conversely, the advantage of Rietveld refinement measurement is that a large number of precipitates are sampled in the residue versus a significantly smaller number measured directly by SEM.

The Nb composition predicted for the nano-sized precipitates compares reasonably well with the mean composition measured using EDX analysis for both the X70 and TWX70 steels (Table 6). However, the Ti composition is under-predicted, and the Mo level is over-predicted when compared with the finest (i.e., 4.2 nm and 5.1 nm) Rietveld refinement predicted precipitates. This difference may be partially attributed to the inclusion of all nano-sized precipitates (including Mo-free ones) in the determination of the mean EDX composition.

The volume percentage of each nano-sized precipitate type predicted by Rietveld refinement (V_f) and the total volume of percentage ($V_{f\text{-}Total}$) of the nano-sized precipitates in each steel are shown in Table 6. The X70 steel exhibits almost double the amount of nano-sized precipitates compared with the TWX70 steel. This difference may be partially attributed to the higher Nb content of the former.

Table 6. Summary of Rietveld refinement and SEM-EDX analysis for nano-sized precipitates.

Steel	Rietveld	EDX Composition (Mean at. Fraction)			R_{QXRD}	R_{SEM}	V_f	$V_{f\text{-}Total}$	σ_{ppt}
		Nb	**Ti**	**Mo**	**(nm)**	**(nm)**	**(%)**	**(%)**	**(MPa)**
X70	$Nb_{0.68}Mo_{0.30}Ti_{0.02}C$	0.79	0.16	0.05	4.2	7.95	0.066	0.113	135.1
	$Nb_{0.85}Ti_{0.15}C$				15.6	-	0.047		
TWX70	$Nb_{0.62}Mo_{0.36}Ti_{0.02}C$	0.66	0.18	0.16	5.1	4.4	0.039	0.064	133.2
	$Nb_{0.84}Ti_{0.16}C$				11.1	10.0	0.025		

4.3. Large Precipitates

Table 7 shows the volume fractions (%) for each composition of large precipitates in X70 and TWX70 steels and the total volume fraction. The total volume fraction calculated by Rietveld refinement for large precipitates in TWX70 steel is almost twice as high (0.070%) as the volume fraction for large precipitates in X70 steel (0.037%). Since large N-rich precipitates would form primarily during casting and subsequent cooling, it is postulated that the difference in the amount of large precipitates between the X70 and TWX70 steels is a result of the casting process.

Table 7. QXRD large precipitate summary for X70 and TWX70 steels.

Steel	Atomic Composition	V_f (%)	Total V_f (%)
X70	$Ti_{0.97}Nb_{0.03}N_{0.68}C_{0.32}$	0.017	0.037
	$Ti_{0.86}Nb_{0.14}N_{0.88}C_{0.12}$	0.004	
	$Ti_{0.64}Nb_{0.36}N$	0.007	
	$Ti_{0.50}Nb_{0.50}N$	0.002	
	$Ti_{0.30}Nb_{0.70}N$	0.007	

Table 7. *Cont.*

Steel	Atomic Composition	V_f (%)	Total V_f (%)
TWX70	$Ti_{0.86}Nb_{0.14}N$	0.028	0.070
	$Ti_{0.84}Nb_{0.16}N$	0.009	
	$Ti_{0.61}Nb_{0.39}N_{0.63}C_{0.37}$	0.009	
	$Ti_{0.50}Nb_{0.50}N_{0.78}C_{0.22}$	0.009	
	$Ti_{0.32}Nb_{0.68}N$	0.016	

5. Conclusions

1. N_2 injection during dissolution minimized/prevented the formation of amorphous SiO_2 during the dissolution process.
2. Rietveld refinement provided reasonably accurate nano precipitate atomic compositions and size values in the X70 microalloyed steels. These results were confirmed by direct SEM-EDX and ICP measurements.
3. Similar types of precipitates (Ti/N-rich, Nb/C-rich, and Nb/Mo/C-rich) were detected in both X70 and TWX70 steels.
4. Nano-sized precipitates with higher Mo levels and lower Nb levels were observed in the TWX70 steel. The presence of the higher Mo content nano-sized precipitates is attributed to the higher Mo content and lower Nb content in the TWX70 steel.
5. Nano-sized precipitates in the thin-walled X70 steel were present in a higher volume fraction (0.113%) than in the thick-walled TWX70 steel (0.064%). This difference is consistent with a higher Nb content in the X70 steel versus the TWX70 steel.

Author Contributions: C.C. completed this work as part of an M.Sc. Degree and was involved in all aspects of producing the work presented in this paper. J.B.W., D.G.I. and H.H. contributed to the conceptualization, analysis, and writing of this paper. The latter two authors also provided formal supervision of C.C.

Conflicts of Interest: The authors declare no conflicts of interest.

Abbreviations

The following abbreviations are used in this manuscript:

QXRD	Quantitative X-ray diffraction
ICP	Inductively coupled plasma mass spectrometry
EDX	Energy dispersive X-ray spectroscopy
SEM	Scanning electron microscopy
TEM	Transmission electron microscopy
TWX70	Thick-walled (17 mm) X70 steel

References

1. Collins, L. Processing of Nb-Containing Steels by Steckel Mill Rolling. In Proceedings of the Niobium Science and Technology: Proceedings of the International Symposium Niobium, Orlando, FL, USA, 2–5 December 2001; pp. 527–542.
2. Bai, D.; Cooke, M.; Asante, J.; Dorricott, J. Process for Making High Strength Micro-Alloy Steel. U.S. Patent US 6,682,613, 27 January 2004.
3. Lu, J. Quantitative Microstructural Characterization of Microalloyed Steels. Ph.D. Thesis, University of Alberta, Alberta, AB, Canada, 2009.

4. Liu, F.; Wang, J.; Liu, Y.; Misra, R.; Liu, C. Effects of Nb and V on microstructural evolution, precipitation behavior and tensile properties in hot-rolled mo-bearing steel. *J. Iron Steel Res. Int.* **2016**, *23*, 559–565. [CrossRef]

5. Kutz, M. *Handbook of Materials Selection*; John Wiley and Sons Inc.: New York, NY, USA, 2002; p. 44.

6. Gladman, T. *The Physical Metallurgy of Microalloyed Steels*; The Institute of Materials: London, UK, 1997.

7. Elwazri, A.M.; Varano, R.; Siciliano, F.; Bai, D.; Yue, S. Characterisation of precipitation of niobium carbide using carbon extraction replicas and thin foils by FESEM. *Mater. Sci. Technol.* **2006**, *22*, 537–541. [CrossRef]

8. Wiskel, J.; Ivey, D.G.; Henein, H. The Effects of Finish Rolling Temperature and Cooling Interrupt Conditions on Precipitation in Microalloyed Steels Using Small Angle Neutron Scattering. *Metall. Mater. Trans. A* **2008**, *39B*, 116–124. [CrossRef]

9. Staron, P.; Jamnig, B.; Leitner, H.; Ebner, R.; Clemens, H. Small-angle neutron scattering analysis of the precipitation behavior in a maraging steel. *J. Appl. Crystallogr.* **2003**, *36*, 415–419. [CrossRef]

10. Perrard, F.; Deschamps, A.; Maugis, P. Modelling the precipitation of NbC on dislocations in ferrite. *Acta Mater.* **2007**, *55*, 1255–1266. [CrossRef]

11. Wiskel, J.; Lu, J.; Omotoso, O.; Ivey, D.; Henein, H. Characterization of Precipitates in a Microalloyed Steel Using Quantitative X-ray Diffraction. *Metals* **2016**, *6*, 90. [CrossRef]

12. Lu, J.; Wiskel, J.; Omotoso, O.; Henein, H.; Ivey, D. Matrix dissolution techniques applied to extract and quantify precipitates from a microalloyed steel. *Metall. Mater. Trans. A* **2011**, *42*, 1767–1784. [CrossRef]

13. Rietveld, H. Line profiles of neutron powder-diffraction peaks for structure refinement. *Acta Crystallogr.* **1967**, *22*, 151–152. [CrossRef]

14. Rietveld, H. A profile refinement method for nuclear and magnetic structures. *J. Appl. Crystallogr.* **1969**, *2*, 65–71. [CrossRef]

15. Popa, N.; Balzar, D. An analytical approximation for a size-broadened profile given by the lognormal and gamma distributions. *J. Appl. Crystallogr.* **2002**, *35*, 338–346. [CrossRef]

16. Balzar, D.; Audebrand, N.; Daymond, M.R.; Fitch, A.; Hewat, A.; Langford, J.I.; Bail, A.L.; Louer, D.; Masson, O.; McCowan, C.N.; et al. Size–strain line-broadening analysis of the ceria round-robin sample. *J. Appl. Crystallogr.* **2004**, *37*, 911–924. [CrossRef]

17. *Standard Test Method for Acid-Insoluble Content of Copper and Iron Powders*; ASTM International: West Conshohocken, PA, USA, 2015.

18. Chatelier, C. Precipitation Analysis in Microalloyed X70 Steels and Heat Treated L80 and T95 Steels. Master's Thesis, University of Alberta, Alberta, AB, Canada, 2017.

19. Coelho, A. *Topas Academic Version 4.1*; Software for Analysis of Powder Diffraction Data; Coelho Software: Brisbane, Australia, 2007.

20. Toby, B. R factors in Rietveld analysis: How good is good enough? *Powder Diffr.* **2006**, *21*, 67–70. [CrossRef]

21. Hill, R.; Howard, C. Quantitative phase analysis from neutron powder diffraction data using the Rietveld method. *J. Appl. Crystallogr.* **1987**, *20*, 467–474. [CrossRef]